Inorganic Chemistry

ARTICLE

pubs.acs.org/IC

Fluoride-Conversion Synthesis of Homogeneous Actinide Oxide Solid Solutions

G. W. Chinthaka Silva,*[,†,‡] John D. Hunn,[‡] Charles Yeamans,[§] Gary S. Cerefice,[†] and Ken R. Czerwinski[†]

[†]Harry Reid Center for Environmental Studies, University of Nevada, Las Vegas, Box 454009, 4505 Maryland Parkway, Las Vegas, Nevada 89154, United States

[‡]Nuclear Fuel Materials Group, Oak Ridge National Laboratory, Oak Ridge, Tennessee 37831-6093, United States

[§]Department of Nuclear Engineering, University of California, Berkeley, 1140 Etcheverry Hall, M.C. 1730, Berkeley, California 94720-1730, United States

ABSTRACT: The synthesis of $(U,Th)O_2$ solid solutions at a relatively low temperature of 1100 °C using a new technique is described. First, separate actinide oxides were reacted with ammonium hydrogen fluoride to form ammonium actinide fluorides at room temperature. Subsequently, this fluoride was converted to an actinide oxide solid solution using a two-phase reaction process, which involved heating of the fluoride first at 610 °C in static air followed by heating at 1100 °C in flowing argon. Oxide solid solutions of UO_2 and ThO_2 were synthesized for a ThO_2 content from 10 to 90 wt %. Microscopic investigation showed that the $(U,Th)O_2$ solid solutions synthesized using this method had high crystallinity and homogeneity up to nanoscale.

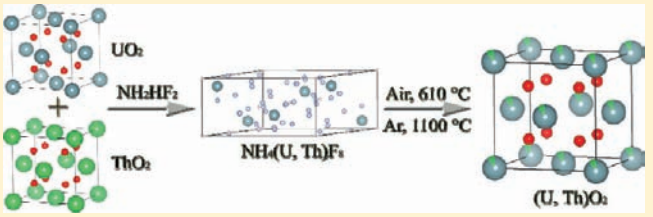

INTRODUCTION

With the inevitable increase in demand for new electrical generating stations, both to replace existing plants at the end of their life cycle and to expand the total generation capacity, nuclear power generation is again being seen as an economically and socially viable option. In the United States alone, the electrical power generated by nuclear plants was over 20% of the total in 2009,[1] with that fraction set to rise in the future as the Energy Policy Act of 2005 implements loan guarantees for new reactor construction. Looking to this potential growth in nuclear energy, mixed thorium−uranium oxide fuels may offer significant advantages compared to traditional uranium oxide fuel, including increased burnup and increased proliferation resistance.[2] Additionally, thoria-based nuclear fuels provide for better performance as a waste form in the direct disposal of the irradiated thoria-based oxide fuels because of high aqueous corrosion resistance[3−5] and reduced leaching rates under oxidizing conditions.[6,7] Thoria-based fuels also provide an attractive option for the transmutation of plutonium and other actinides[8] because of their crystal structures, which are analogous to other tetravalent actinide oxides. Fabrication of mixed oxide (solid solutions) fuels with a suitable degree of homogeneity currently requires high temperature. Any chemical synthesis technique that reduces the temperature would make the overall fabrication process easier and more energy-efficient. The use of a novel route, possibly to lessen such a burden in the synthesis of oxide solid-solution fuel materials, is discussed here.

Current synthetic routes for actinide oxide solid solutions require significant time and effort to produce a well-homogenized mixed oxide product. Two synthetic routes are commonly used for the synthesis of actinide oxide solid solutions: dry pyroprocessing and wet aqueous coprecipitation. In the dry method, the separate actinide oxides are mixed and heated to 1700 °C or higher under reducing atmospheric conditions[9,10] for 48 h or more. Even after this prolonged synthesis, the resulting products often fail to meet the required degree of homogeneity, requiring the product to be milled or ground and resintered, sometimes more than once, to produce a final product that meets the requirement. In the wet method, the actinides are dissolved in an aqueous system and coprecipitated. The resulting precipitate is converted to oxide at 1650 °C under a reducing atmosphere to form the final actinide oxide solid solution.[11] Literature has shown the ability to use such wet methods to fabricate actinide oxide solid solutions at comparatively low temperatures such as 1300[12] and 1200 −1400 °C.[13] These wet methods use precursor precipitates such as crystals of mixed actinide hydroxides[13] and oxalates[14] for final oxide solid solutions. These precursors have the advantage of suitable particle and surface characteristics such as crystallite size, surface area, and homogeneity for compaction toward a final fuel material together with control of the sintering temperature with given precursor characteristics.[15,16]

One of the uses of mixed oxide solid solutions is the transmutation of plutonium and other minor actinides produced in the fuel cycle. These transuranics have high vapor pressures and therefore high volatility at elevated temperatures.[17] Therefore, it is imperative to have alternative techniques to synthesize actinide oxide solid solutions at lower temperatures. An alternative approach to the coprecipitation method is the sol−gel wet method. The sol−gel method requires lower synthesis temperatures than those used by either the dry or coprecipitation method. However, the

Received: July 20, 2011
Published: October 13, 2011

sol−gel method requires a complicated synthetic process: sol preparation, gelation, washing, drying, heat treatment at 300 °C for 3 h, humidification, pelletization, and heating at 1100 °C in an Ar/H_2 atmosphere for 2−3 h in order to obtain the oxides.[18]

In this current study, a versatile, low-temperature fluoride route for fabricating actinide oxide solid solutions is presented. The UO_2/ThO_2 system was tested, varying the amount of ThO_2 incorporated into the UO_2 solid matrix. A series of ammonium actinide fluoride samples of uranium and thorium were made by reacting mixed oxides of UO_2 and ThO_2 (10−90 wt %) with excess NH_4HF_2. These fluorides were then heat-treated to synthesize the terminal oxide solid solutions. This method, developed and tested for the $(U,Th)O_2$ system, also has potential application for the higher actinides.

MATERIALS AND METHODS

Ammonium Uranium−Thorium Fluoride [$(NH_4)_4U_{1-x}Th_xF_8$] Synthesis. Solid powders of UO_2 and ThO_2 (International Bio-Analytical Industries, Inc.) were mixed using different weight ratios and changing the ThO_2 amount from 10 to 90 wt %. Solid NH_4HF_2 was added to the uranium−thorium oxide powder in a 4:1 stoichiometric molar ratio, with an additional excess of 10% in NH_4HF_2, and the resulting mixture was mixed using a mortar and pestle for approximately 10 min. The expected reaction that evolves in this fabrication is as follows:

$$(1-x)UO_2(s) + xThO_2(s) + 4NH_4HF_2(s) \rightarrow (NH_4)_4U_{1-x}Th_xF_8(s) + 2H_2O(l)$$

The resulting powder samples were transferred into polyethylene vials and sealed for 2 days in order to ensure that conversion of the oxide to the ammonium fluoride salt was complete before using the samples for the next step.

Heat Treatment of the Ammonium Uranium−Thorium Fluorides. Heat treatment of the resulting ammonium fluorides of mixed uranium and thorium was done inside a quartz tube. Because the reactant ammonium actinide fluorides consisted of fine powder, no additional grinding was performed. The samples were placed on a platinum foil and inserted into the quartz tube. Both ends of the quartz tube were sealed and attached to gas stream tubing. All heat treatments were carried out up to a maximum temperature of 1100 °C at a 9 °C/min heating rate and held at 1100 °C for 30 min. The atmosphere consisted of either air, argon, or Ar/H_2. Oxide solid solutions were made using a two-step reaction: conversion of the reactants into oxide under static air and completion of the conversion under an inert atmosphere. Further details are reported in the Results section, and the use of different experimental conditions (heating time, temperature, and cover gas) is also discussed at the end of this article. Following are two possible reactions for this conversion, assuming a terminal product of $U_{1-x}Th_xO_2(s)$.

$$(NH_4)_4U_{1-x}Th_xF_8(s) + O_2(g) \xrightarrow{\text{air, 610 °C; Ar, 1100 °C, 30 min}} U_{1-x}Th_xO_2(s) + 4NH_4F(s) + 2F_2(g)$$

$$(NH_4)_4U_{1-x}Th_xF_8(s) + 2H_2O(l) \xrightarrow{\text{air, 610 °C; Ar, 1100 °C, 30 min}} U_{1-x}Th_xO_2(s) + 4NH_3(g) + 8HF(g)$$

XRD Measurements. Powder X-ray diffraction (XRD) patterns of the reactant fluorides and product oxides were obtained using Cu Kα radiation. The current and voltage used were 40 mA and 40 kV, respectively. A LaB_6 SRM 660a NIST internal standard was admixed with the samples before acquisition of the powder XRD patterns. Lattice parameters were refined by the Rietveld method using TOPAS academic[19] and GSAS[20] programs.

Table 1. Sample Compositions and the Products Formed after Reaction with NH_4HF_2

wt %		
UO_2	ThO_2	terminal products
90	10	$(NH_4)_4U_{0.9}Th_{0.1}F_8$
80	20	$(NH_4)_4U_{0.8}Th_{0.2}F_8$
70	30	$(NH_4)_4U_{0.7}Th_{0.3}F_8$
60	40	$(NH_4)_4U_{0.6}Th_{0.4}F_8$
50	50	$(NH_4)_4U_{0.5}Th_{0.5}F_8$
40	60	$(NH_4)_4U_{0.4}Th_{0.6}F_8$
30	70	91% $(NH_4)_4U_xTh_{1-x}F_8$/ 9% $(NH_4)_4ThF_8$ and/or $(NH_4)_4UF_8$
20	80	61% $(NH_4)_4U_xTh_{1-x}F_8$/ 39% $(NH_4)_4ThF_8$ and/or $(NH_4)_4UF_8$
10	90	74% $(NH_4)_4U_xTh_{1-x}F_8$)/ 26% $(NH_4)_4ThF_8$ and/or $(NH_4)_4UF_8$

Microscopic Measurements. The microstructures of the resulting oxide solid-solution samples were studied by transmission electron microscopy (TEM) at high resolution. Elemental mapping was carried out using electron energy-loss spectrometry (EELS). A Tecnai-G2-F30 supertwin TEM system with a 300-keV Schottky field-emission gun was used in these characterizations. All TEM images were recorded using a slow-scan CCD camera attached to a Gatan GIF 2000 energy filter. Kinematical electron diffraction and high-resolution TEM (HRTEM) simulations[21] were also used to support HRTEM imaging.

TEM Specimen Preparation. Microtome cutting was used in TEM specimen preparation: several milligrams of sample were mixed with spur resin in a microvial. This mixture was solidified by drying at 60 °C overnight. The spur resin used for these samples was a mixture of 10.0 g of vinylcyclohexene dioxide, 4.0 g of a diglycidyl ether of poly (propylene glycol), 26.0 g of nonenylsuccinic anhydride, and 0.4 g of (dimethylamino) ethanol. The sample embedded in the resin was cut into slices with a thickness of 20−50 nm using a Leica EM UC6rt microtome. The resulting samples were loaded onto a 3-mm copper grid for TEM analysis.

RESULTS

Synthesis and Characterization of Ammonium Actinide Fluorides. The synthesis method investigated for $(U,Th)O_2$ solid solutions from the corresponding actinide oxides by a solid-phase low-temperature fluoride route consisted of two main steps. In the first step, nine different solid mixtures of UO_2 and ThO_2 with excess ammonium hydrogen fluoride were made by varying the ThO_2 amount from 10 to 90 wt % with 10 wt % increments. Solid solutions of $(NH_4)_4U_{1-x}Th_xF_8$ formed at a thorium content up to 60 wt % (Table 1). The raw products contained some impurity peaks, especially at low 2θ angles such as at 12.6°, 16.2°, and 17.2° in their powder XRD patterns (Figure 1, lower pattern). However, sample drying at 80 °C diminished or removed most of these impurity peaks (Figure 1, upper pattern), suggesting that they were probably due to ammonium fluoride and/or unreacted ammonium hydrogen fluoride residue in the samples. A decrease of these impurity peaks, by heating the crude products at low temperatures, suggested that the presence of these fluoride impurities did not

dx.doi.org/10.1021/ic201552g |Inorg. Chem. 2011, 50, 11004–11010

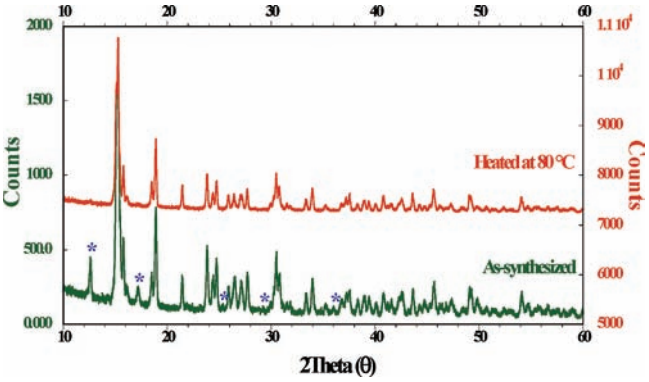

Figure 1. Powder XRD patterns of the $(NH_4)_4U_{1-x}Th_xF_8$ solid solutions, where x = 0.6. The two patterns represent the sample as-synthesized and after drying at 80 °C. Some of the impurity peaks, possibly due to incompletely reacted or extra ammonium fluorides, are highlighted.

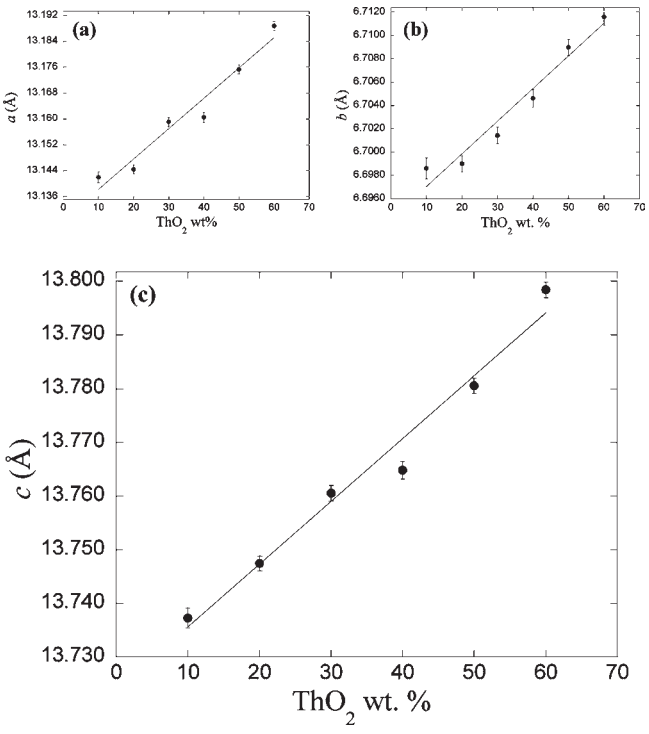

Figure 2. Lattice parameter variation of the monoclinic $(NH_4)_4U_{1-x}Th_xF_8$ (space group $C2/c$) as a function of the ThO_2 weight percentage in the first six samples in Table 1: (a) variation in a; (b) variation in b; (c) variation in c.

affect the terminal target materials with respect to their chemical compositions or other significant chemical characteristics.

For the single-phase systems, the impact of the initial ThO_2 weight percentage on the lattice parameter of the product ammonium actinide fluoride is shown in Figure 2. All a, b, and c lattice parameters increase linearly with respect to an increase in the thorium level up to 60 wt % thorium, confirming the solid-solution behavior according to Vegard's law to be within the accuracy of the measurement.[22,23] While these six samples contained ammonium actinide fluoride solid solutions of a general chemical composition of $(NH_4)_4U_{1-x}Th_xF_8$, two separate phases

Table 2. Two-Step Conversions of $(NH_4)_4U_{0.6}Th_{0.4}F_8$ up to 1100 °C under Static Air/Flowing Argon

	chemical phases in the product	
Ar flow initiation temperature (°C)	primary	secondary
870	UO_2	ThO_2
820	ThO_2	UO_2 and U_3O_8
710	SS[a]	
610	SS[a]	

[a] SS = solid solution.

Table 3. Results Obtained for the Heating of $(NH_4)_4U_{0.9}Th_{0.1}F_8$ under Air[a]

		products		
temperature (°C)	time (min)	primary	secondary	impurity peaks
550	30	UF_4	UO_2F_2, U_3O_8	
800	30, 60	ThF_4	U_3O_8, SS, ThO_2	
900	30	U_3O_8	SS, ThO_2	yes
1000	30	U_3O_8	SS, ThO_2	yes
1100	30	SS		

[a] SS = solid solution.

formed at higher thorium content ($x \geq 0.7$). Powder XRD refinement was done by fitting the two-phase pattern to the ammonium actinide fluoride solid-solution and single ammonium actinide fluoride phases. Some of the peaks in the XRD patterns overlapped in such a way as to make positive identification of the pure phase [$(NH_4)_4ThF_8$ and $(NH_4)_4UF_8$] unreliable. The majority of the phases of these three samples were the fluoride solid solution. For a 90 wt % thorium sample, the second phase was probably $(NH_4)ThF_8$. Given the experimental conditions (reaction of the oxides with NH_4HF_2 for 2 days at ambient conditions) used to synthesize the fluorides, the single ammonium actinide fluoride phase behavior and the linear variation of the lattice parameters in samples up to 60 wt % ThO_2 suggest up to 60 wt % thorium incorporation into the $(NH_4)_4U_{1-x}Th_xF_8$ system. According to the phase weight percentages of the last three samples, one further proposes an upper limit of 66.6 wt % thorium incorporation into the ammonium actinide fluoride solid solution. Even though two-phase fluorides were present in these last three samples, as is shown in the following sections, the presence of either a single ammonium actinide fluoride phase or a polyphase in the reactants did not affect the formation of the expected oxide solid solution.

Synthesis and Characterization of the (U,Th)O_2 Oxide Solid Solution. The optimized experimental conditions for synthesis of the oxide solid solutions contained a two-step reaction path. First, the ammonium actinide fluoride samples were heated in an air-filled quartz tube under static flow conditions to a target temperature of 610 °C. This was done to prevent any removal of high-vapor-pressure fluorides with flowing gas conditions. In the second step, an argon flow at 610 °C over the sample was initiated and maintained throughout the remainder of the reaction at a final temperature. Argon flow at the second stage was necessary to hinder further oxidation of the tetravalent actinide oxide solid solutions into U_3O_8 with higher oxidation

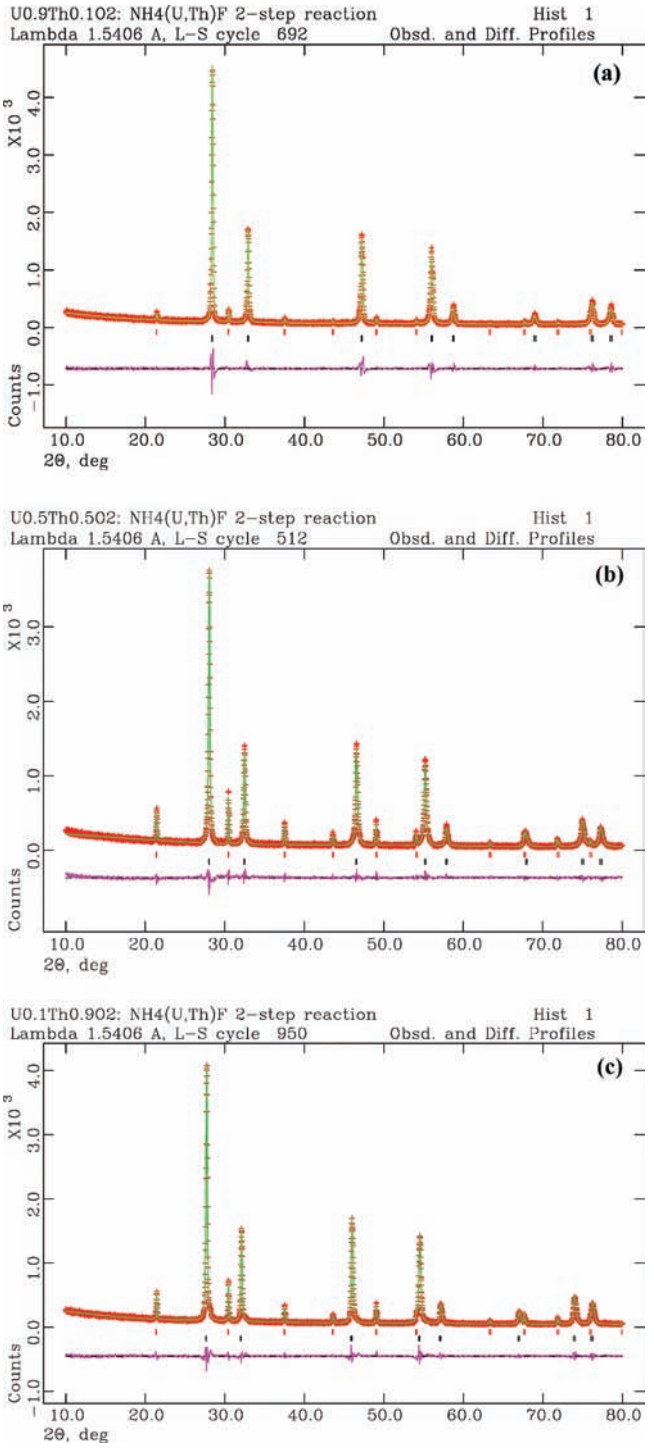

Figure 3. Powder XRD analysis of three representative $(U,Th)O_2$ solid-solution samples: (a) $U_{0.9}Th_{0.1}O_2$ (CHI**2 = 1.844); (b) $U_{0.5}Th_{0.5}O_2$ (CHI**2 = 1.362); (c) $U_{0.1}Th_{0.9}O_2$ (CHI**2 = 1.322). Experimental (red), calculated (green), and residual (pink) patterns are shown. Lower tick marks (black) represent the oxide phase.

states (V and VI). A temperature of 610 °C was used for the first step of the reaction because it was the lowest argon initiation temperature that produced the expected single-phase oxide solid solution among the other temperatures tested (870, 820, and 710 °C) for the $(NH_4)_4U_{0.6}Th_{0.4}F_8$ reactant (Table 2). At 870 and 820 °C, two (UO_2 and ThO_2) and three (UO_2, ThO_2, and a

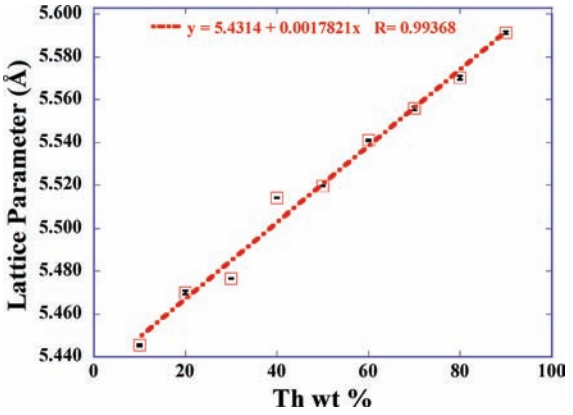

Figure 4. Lattice parameter variation of the $(U,Th)O_2$ solid solutions as a function of the thorium weight percentage. The error associated (<0.009%) with the refined lattice parameters is also plotted.

small amount of U_3O_8) chemical phases were observed, respectively. The expected oxide solid solution was obtained at both 710 and 610 °C. A temperature of 610 °C was used instead of 710 °C for two reasons: to reduce the formation of other higher oxides (Tables 2 and 3) and to reduce the removal of product fluorides/unreacted fluoride reactants due to argon gas flow (static conditions were used in the first part of the reaction), as discussed later in the paper. The presence of a small amount of U_3O_8 in the sample where argon flow was initiated at 820 °C compared to 870 °C might have been observed because of slight variations in the experimental conditions. The main observation here, however, is that 820 and 870 °C temperatures were not low enough to initiate the inert atmospheric conditions so that further oxidation of the terminal oxide phase would be inhibited.

The use of optimized experimental conditions (two-step process: heat treatment up to 610 °C under static air and up to 1100 °C under flowing argon) for fluoride samples covering the full composition range from 10 to 90 wt % thorium produced the expected single-phase oxide solid solution. Three examples of XRD/Rietveld analyses of three oxide samples are shown in Figure 3. The lattice parameters of these oxide solid solutions are plotted against the thorium weight percentage in the samples in Figure 4. The lattice parameter increases linearly with respect to an increase in the thorium weight percentage incorporated into the oxide matrix with a correlation coefficient of 0.99, indicating a good resemblance to Vegard's law within the accuracy of the measurement. This variation further confirmed the formation of a complete series of single-phase $U_{1-x}Th_xO_2$ solid solutions for $0.1 \leq x \leq 0.9$ compositions tested.

Samples were also examined by TEM to explore the homogeneity and microstructure. Elemental mapping obtained for $U_{0.9}Th_{0.1}O_2$ is shown in Figure 5. Uranium and thorium elemental maps show a uniform distribution throughout the particle cluster. The elemental signals appear more prominent at the particle edges as an artifact of variations in the particle thickness. The oxygen elemental map also shows a uniform distribution. The uniform elemental distribution of uranium, thorium, and oxygen throughout the particles is an indication of a single-phase homogeneous solid solution.

HRTEM images showed the presence of highly crystalline particle areas in the as-synthesized oxide solid solution samples. Figure 6a shows a typical example, where high crystallinity was observed in $U_{0.9}Th_{0.1}O_2$. The well-resolved different spots in the

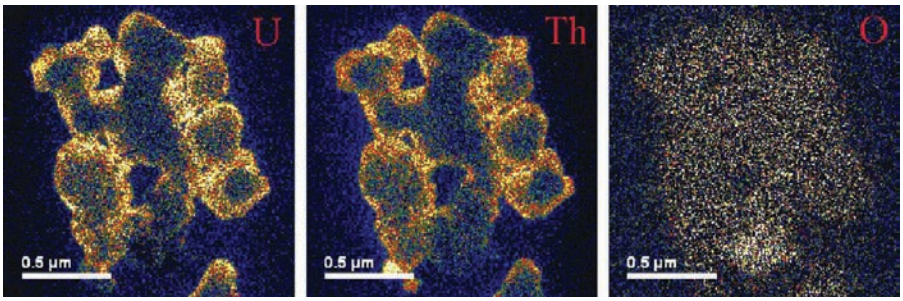

Figure 5. Uranium, thorium, and oxygen EELS elemental maps of the $U_{0.9}Th_{0.1}O_2$ sample.

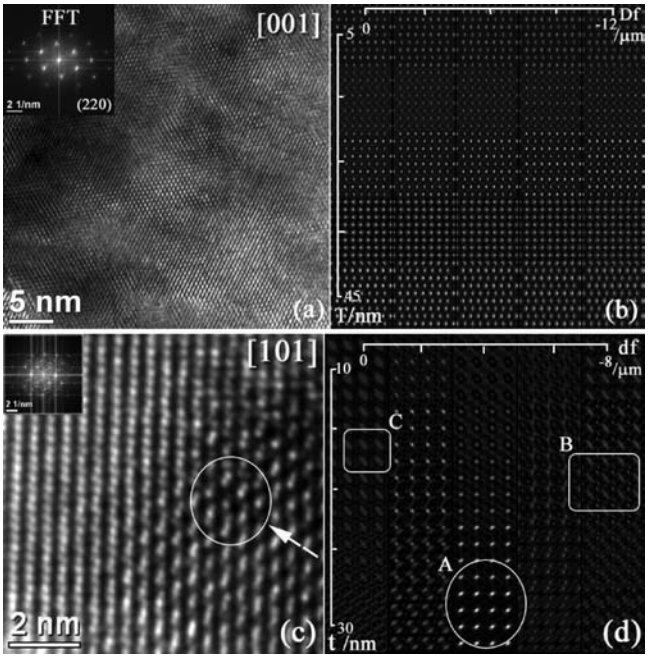

Figure 6. HRTEM microscopic images of $U_{0.9}Th_{0.1}O_2$ solid solutions. (a) HRTEM image of a crystalline particle area of the sample. (b) Bloch simulation of the oxide corresponding to the (220) reflection along the [001] zone with respect to different thicknesses and defocuses. (c) Detail of another particle area. (d) Bloch simulation of the oxide due to (111) planes along the [101] zone at different values of thickness and defocus.

corresponding fast Fourier transform micrograph (Figure 6a, inset) also indicate the resolution of the oxide phase lattice fringes, confirming the high crystallinity of the particle area. Furthermore, the lattice fringes were comparable to the oxide phase *d* spacing of (220) lattice planes. With given thickness and defocus values, the calculated lattice fringe details assuming (220) reflection along the [001] zone axis depicted in Figure 6b also confirm the lattice orientation of the oxide phase observed in Figure 6a. A 2-fold order was seen in lattice fringes of another particle area, as shown in Figure 6c. These lattice fringes correspond to the (111) lattice plane of the oxide phase. An area containing more separated lattice fringes compared to the rest of the lattice fringes in Figure 6c is highlighted by a circle. If they came from separate uranium or thorium oxide phases, these lattice fringes should have an ordered appearance, as indicated by a circle in the calculated lattice fringe pattern in Figure 6d. If the 2-fold order was a result of the thickness or defocus variance, then

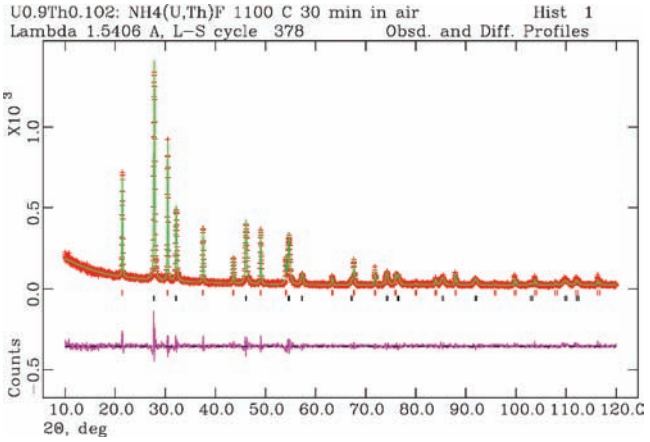

Figure 7. Rietveld/XRD analysis of the $U_{0.9}Th_{0.1}O_2$ solid solution synthesized by heating of the reactant fluoride at 1100 °C for 30 min under air. Reduced CHI**2 = 1.220. Lower tick marks represent the oxide phase.

the fringe details should be similar to those in the areas highlighted by rectangles in Figure 6d. The presence of both closely packed and comparatively separated lattice fringes of this high-magnification oxide nanostructure image in Figure 6d further verified the incorporation of thorium into the oxide solid solution.

DISCUSSION

Initial studies performed here on a single-step synthesis of $(U,Th)O_2$ solid solutions by heating of the ammonium actinide fluorides under air and argon produced multiple-phase samples. Under air, a complete conversion of the ammonium actinide fluoride into the corresponding oxide solid solution was observed only after heating of the reactant up to the maximum available furnace temperature of 1100 °C for 30 min (Table 3). Rietveld refinement of the XRD pattern of that as-synthesized solid solution is shown in Figure 7. Even though a second oxide phase could not be fitted into the XRD pattern, considerable residual peak intensities, especially at ~27.8°, may be an indication of the formation of a second oxide phase at 1100 °C even up to a minimum temperature holding time of 30 min when air was used as the cover gas. The absence of enough information in the XRD pattern, which is, in fact, the case in most XRD pattern fittings, to obtain a good fit in the refinement is also a possible reason for such residual peak intensities. As shown in this table, prolonged heating of the reactant fluorides even at low temperatures such as 800 °C could result in further oxidation of the expected terminal

dx.doi.org/10.1021/ic201552g |*Inorg. Chem.* 2011, 50, 11004–11010

Table 4. Heat Treatment of the Samples at 1100 °C for 30 min under Air[a]

	products		
Th wt %	primary	secondary	U_3O_8 wt %
10	U_3O_8	SS	83.7
20	U_3O_8	SS, ThO_2	61.1
30	SS	U_3O_8, ThO_2	48.8
40	SS	U_3O_8, ThO_2	34.2
50	SS	U_3O_8, ThO_2	22.1
60	SS		
70	SS	U_3O_8	0.9
80	SS	U_3O_8, UO_2 (25.1)	1.1
90	SS		

[a] SS = solid solution.

oxide phase. Therefore, a minimum holding time of 30 min was used.

These experimental conditions, heating of the reactants at 1100 °C for 30 min under air, were used in all other compositions. Under these experimental conditions, the expected single-phase (U,Th)O_2 solid solutions were observed only with the 60, 70 (with less than 1 wt % U_3O_8 in the product), and 90 wt % thorium-containing samples. All other samples contained significant amounts of secondary oxides such as U_3O_8 and UO_2 (Table 4). The U_3O_8 level decreased with a decrease in the uranium level in the reactants as expected (Table 4). In the first sample (10 wt % ThO_2), all of the reactant thorium has been incorporated into the tetravalent oxide phase, with U_3O_8 being the other and the major chemical phase. As the uranium level in the reactants decreased, the product phase U_3O_8 level decreased and secondary ThO_2 started to form. This indicated that with a decrease in the precursor uranium level the formation of the oxide solid solution is favored, and it was becoming stable to further oxidation into U_3O_8. The formation of ThO_2 also started to decrease as the thorium level in the reactants increased. At 60 wt % thorium, no secondary phase was observed. The 50 wt % thorium could be considered as a turning point, where thorium started to stabilize the oxide solid solution, except for the formation of a considerable amount of UO_2 in the 80 wt % ThO_2 sample. Several attempts to produce a single-phase oxide solid solution for the 80 wt % sample were not successful. Even the 10 wt % thorium-containing sample failed to reproduce the oxide solid solution under the same experimental conditions. These observations suggest an uncontrollable oxidation of the products under air. Reduction of the secondary oxide phases such as U_3O_8 produced separate oxide phases rather than single-phase oxide solid solutions under NH_3(g).

In a second set of experiments, either high-purity argon or Ar/H_2 (4%) was employed as a cover gas to prevent further oxidation of the oxides into U_3O_8. Even though some compositions showed no oxidation into higher oxides, unexpected high weight losses were identified in some of the samples. The fluorides have a relatively low density and a downy bulk texture and thus might have a high susceptibility of being entrained in the cover gas.

To reduce this entrainment problem, a two-step reaction path was developed. In this set of experiments, the ammonium actinide fluoride samples were heated in an air-filled quartz tube under static flow conditions to a target temperature of 610 °C followed by continuation of the reaction under flowing argon up to 1100 °C. Overall, the optimum conditions to synthesize (U,Th)O_2 solid solutions from mixtures of discrete starting oxides were found to be fluorination by ammonium hydrogen fluoride at 25 °C, followed by a two-step decomposition process of the ammonium actinide fluorides to the target (U,Th)O_2 solid solution.

Results obtained for the ammonium actinide fluoride of U/Th = 0.9 chemical composition suggested formation of the expected oxide solid solution and its partial oxidation into U_3O_8 under air (Table 3). The products obtained for the same compound at 1100 °C under air (Table 3) implied decomposition of U_3O_8 into the tetravalent oxide phase. This result, however, could not be reproduced the second time (Table 4) at the same temperature in air, implying that the tetravalent oxide phase was not produced through a U_3O_8 decomposition route. The absence of U_3O_8 in the samples made using inert atmospheric conditions starting at 610 °C through 1100 °C also supported this observation. Thus, it is postulated that ammonium actinide fluorides decompose to first produce the expected tetravalent oxide phase followed by the formation of any secondary U_3O_8 phases if further oxidation is permitted by allowing enough oxygen to be present in the experimental setup.

Hubert et al. showed that a (U,Th)O_2 solid solution can be synthesized using precipitation methods over a composition range of 11−91 atom % uranium, and this was confirmed using Vegard's law.[5] Another study in which $U_{1-x}Th_xO_2$ was synthesized using the sol−gel method also reported holding Vegard's law over the full composition range studied ($0.0 \le x \le 1.0$).[24] In this present work, the decomposition of $(NH_4)_4U_{1-x}Th_xF_8$/$\{(NH_4)_4UF_8 + (NH_4)_4ThF_8\}$ in an air-filled atmosphere up to 610 °C followed by further heating of the material in an inert atmosphere up to 1100 °C produced the expected $U_{1-x}Th_xO_2$ solid solutions for the whole range of thorium content of $0.1 \le x \le 0.9$ tested (Figure 4). Given the isomorphous characteristics of the AnO_2 (An = actinide) structures and proof of the possibility of making a complete series of $U_{1-x}Th_xO_2$ for compositions in the range of $0.0 \le x \le 1.0$, it can be postulated that the current novel route could be used to synthesize (U,Th)O_2 for a whole composition range of $0.0 \le x \le 1.0$ without any limitations. As seen in this study, part of the uranium content in the solid matrix tends to get oxidized at low thorium levels. Therefore, it is expected to form secondary higher oxides for $x <$ 0.1 when this method is used. Further optimization of the temperature used in the first step of the reaction might be needed in obtaining single-phase solid solutions for <10 wt % thorium samples. Future experimentation is expected to cover two extreme ends of the composition range and sintering behavior of the solid solutions made using this fluoride route.

AUTHOR INFORMATION

Corresponding Author

*E-mail: silvagw@ornl.gov. Tel: (865)574-6264. Fax: (865)574-4186.

ACKNOWLEDGMENT

Sample synthesis and characterization was performed at the University of Nevada, Las Vegas (UNLV), under the UNLV Transmutation Research Program and were funded by the U.S. Department of Energy (Grant DE- FG07-01AL67358). Completion of this manuscript and final data analysis at Oak Ridge

National Laboratory (ORNL) was sponsored by the U.S. Department of Energy Office of Nuclear Energy. The authors thank Dr. Anthony Hechanova for administrating the UNLV Transmutation Research Program and Tom O'Dou and Trevor Low for laboratory management and radiation safety support for this work. We thank Dr. Terrence B. Lindemer, retired staff member of ORNL, for valuable discussions that helped to improve the quality of the paper. Many thanks go to Dr. Gary Bell and Dr. Rodney Hunt at ORNL for reviewing the manuscript.

REFERENCES

(1) http://www.world-nuclear.org/info/inf41.html.
(2) Herring, J. S.; MacDonald, P. E.; Weaver, K. D.; Kullberg, C. *Nucl. Eng. Des.* **2001**, *203*, 65–85.
(3) Fourest, B.; Vincent, T.; Lagarde, G.; Hubert, S.; Baudoin, P. *J. Nucl. Mater.* **2000**, *282*, 180–185.
(4) Hubert, S.; Barthelet, K.; Fourest, B.; Lagarde, G.; Dacheux, N.; Baglan, N. *J. Nucl. Mater.* **2001**, *297*, 206–213.
(5) Hubert, S.; Purans, J.; Heisbourg, G.; Moisy, P.; Dacheux, N. *Inorg. Chem.* **2006**, *45*, 3887–3894.
(6) Heisbourg, G.; Hubert, S.; Dacheux, N.; Purans, J. *J. Nucl. Mater.* **2004**, *335*, 5–13.
(7) Hubert, S.; Heisbourg, G.; Dacheux, N.; Moisy, P. *Inorg. Chem.* **2008**, *47*, 2064–2073.
(8) Akie, H.; Muromura, T.; Takano, H.; Matsuura, S. *Nucl. Technol.* **1994**, *107*, 182–191.
(9) Cohen, I.; Berman, R. M. *J. Nucl. Mater.* **1966**, *18*, 77–107.
(10) Eichler, R.; Hanus, D.; Krellmann, J.; Lob, J.; Roepenack, H. *J. Nucl. Mater.* **1984**, *124*, 9–13.
(11) Sari, C.; Benedict, N.; Blank, H. *J. Nucl. Mater.* **1970**, *35*, 267–277.
(12) Heisbourg, G.; Hubert, S.; Dacheux, N.; Ritt, J. J. *Nucl. Mater.* **2003**, *321*, 141–151.
(13) Yildiz, O. *J. Nucl. Mater.* **2007**, *366*, 266–271.
(14) Clavier, N.; Hingant, N.; Rivenet, M.; Obbade, S.; Dacheux, N.; Nicole, B.; Abraham, F. *Inorg. Chem.* **2010**, *49*, 1921–1931.
(15) Hingant, N.; Clavier, N.; Dacheux, N.; Barre, N.; Hubert, S.; Obbade, S.; Taborda, F.; Abraham, F. *J. Nucl. Mater.* **2009**, *385*, 400–406.
(16) Hingant, N.; Clavier, N.; Dacheux, N.; Hubert, S.; Barre, N.; Podor, R.; Aranda, L. *Powder Technol.* **2011**, *208*, 454–460.
(17) Ward, W.; Kleinschmidt, P. D.; Haire, R. G. *J. Chem. Phys.* **1979**, *71*, 3920.
(18) Tel, H.; Eral, M.; Altas, Y. *J. Nucl. Mater.* **1998**, *256*, 18–24.
(19) Coelho, A. A. *J. Appl. Crystallogr.* **2000**, *33*, 899–908.
(20) Larson, A.C.; Von Dreele, R. B. *General Structure Analysis System (GSAS)*; Los Alamos National Laboratory Report LAUR 86-748; Los Alamos National Laboratory: Los Alamos, NM, 2004.
(21) Zuo, J. M. *Microsc. Microanal.* **2004**, *10* (Suppl 2), 84–85.
(22) Vegard, L. *Z. Phys.* **1921**, *5*, 17.
(23) Jenkins, R.; Synder, R. L. *Introduction to X-ray Diffractometry*; John Wiley & Sons, Inc.: New York, 1996; pp 42−43.
(24) Bamberger, C. E.; Baes, C. F. *J. Nucl. Mater.* **1970**, *35*, 177–182.